

A&A manuscript no.
(will be inserted by hand later)

Your thesaurus codes are:
missing; you have not inserted them

ASTRONOMY
AND
ASTROPHYSICS
May 14, 2018

The broad band spectrum and variability of NGC 4151 observed by BeppoSAX

A. De Rosa¹, L. Piro¹, G. C. Perola², M. Capalbi³, M. Cappi⁴, P. Grandi⁴, L. Maraschi⁵, and P. O. Petrucci⁶

¹ Istituto di Astrofisica Spaziale e Fisica Cosmica, INAF, sezione di Roma, Via Fosso del Cavaliere, 00133 Roma, Italy

² Dipartimento di Fisica, Università degli Studi “Roma Tre”, Via della Vasca Navale 84, I-00146 Roma, Italy

³ ASI Science Data Center, c/o ESA-ESRIN, Via Galileo Galilei, 00044 Frascati, Italy

⁴ Istituto di Astrofisica Spaziale e Fisica Cosmica, INAF, sezione di Bologna, Via Gobetti 101, I-40129, Italy

⁵ Osservatorio Astronomico di Brera, INAF, Via Brera 28, Milan I-20121, Italy

⁶ Laboratoire d’Astrophysique de Grenoble, BP 43, 38041 Grenoble Cedex 9, France

Abstract. We present an analysis of all *BeppoSAX* observations of NGC 4151. This source was observed 5 times from 1996 to 2001 with durations ranging from a day to four days. The intrinsic continuum (described as a cut-off power law), is absorbed at low energies by a complex system: a cold patchy absorber plus a warm uniform screen photoionized by the central continuum. We find that this “dual absorber” is the main driver of the observed variability, up to a factor of eight, at 3 keV. In particular the covering fraction of the cold absorber changes on time scales of the order of a day, supporting its association with the Broad Line Region. The column density of the warm gas varies on a longer time scale (months to year). Some of the small amplitude spectral variability above 10 keV can be explained with an intrinsic variation (with variation of the photon index $\Delta\Gamma \sim 0.2$). The flux below 1 keV remains constant confirming an extended origin. Its spectrum is reproduced by a combination of a thermal component (with temperature $kT = 0.15$ keV) and a power law with the same slope as the intrinsic continuum but with an intensity a few per cent. A Compton reflection component is significantly detected in 1996 (averaged value of $\Omega/2\pi \sim 0.4$, with Ω the solid angle covered by the reflecting medium), with intensity decreasing on time scale of year, and it disappears in 2000 and 2001. The long time scale of variations argues for an association with an optically thick torus at a distance of few light years. An iron line was detected in all spectra. Its energy is consistent with fluorescence by cold iron. We find that the line is variable. Its behaviour is reproduced by a variable component proportional to the level of the reflection flux plus a constant component. The flux of the latter is consistent with the extended line emission observed by *Chandra*. We conclude that the first component is likely arising from the

torus and the second is produced in the extended Narrow Line Region.

Key words: Galaxies: Seyfert; X-rays: galaxies; Galaxies: individual: NGC 4151

1. Introduction

The Seyfert galaxy NGC 4151 is one of the brightest AGN. It has been considered for years the prototype of its class and, as such, has been extensively studied at all wavelengths (see Ulrich 2000 for a review). In X-rays its spectrum is the most complex observed so far in AGN, being characterized by narrow and broad spectral features from soft to hard X-rays (e.g. Perola et al. 1986; Zdziarski et al. 1996; Zdziarski et al. 2002). The central X-ray continuum is absorbed below a few keV by a (complex) absorber with column density $N_H \approx 10^{23} \text{ cm}^{-2}$ associated with the Broad Line Region (BLR, Reichert, Mushotzky & Holt 1986). This absorption in NGC 4151 allows to reveal the presence of soft X-ray components below 1 keV, associated with a scattering component and a thermal plasma with a low temperature of ~ 0.1 keV (Perola et al. 1986; Pounds et al. 1986; Weaver et al. 1994b) as those observed in type 2 objects (e.g. Antonucci 1993; Matt et al. 1997).

At higher energies NGC 4151 shows an iron line which remains remarkably constant notwithstanding large variations of the continuum (Perola et al. 1986; Schurch et al. 2003). Observations by *Chandra* (Ogle et al. 2000) have indeed shown that most of the line is produced in the Narrow Line Region (NLR). The iron line site of Seyfert 1 galaxies has often been associated in the past with an accretion disk (e.g. Tanaka et al. 1995; Fabian et al. 2000). *XMM-Newton* and *Chandra* observations have shown that a

narrow line component is a common feature in Sy 1s (Reeves et al. 2001; Pounds et al. 2001; Matt et al. 2001; Kaspi et al. 2001). Further insight on the nature of the reprocessing medium should also become available through measurements of the reflection component. Recent *INTEGRAL* observation (Beckmann et al. 2005) described the hard X-ray/soft-gamma spectrum of NGC 4151 with a Compton continuum from hot electrons ($kT_e \simeq 100$ keV) in an optically thick ($\tau=1.3$) corona plus a reflected component from a cold material subtending a solid angle of $\Omega/2\pi \simeq 0.7$.

NGC 4151 has been one of the first Seyfert 1 galaxy with a well established evidence of changes of the spectral index correlated with the luminosity (Perola et al. 1986; Yaqoob et al. 1993). With the increased bandwidth and sensitivity of present instrumentation, this feature appears to be present in other Seyfert 1 galaxies (e.g. 1H 0419-577, Page et al. 2002; NGC 3783, De Rosa et al. 2002; MCG-6-30-15, Vaughan & Edelson 2001; NGC 5548, Petrucci et al. 2000, Nicastro et al. 2000; NGC 7469, Nandra et al. 2000; IC 4329A, Done et al. 2000; Mkn 509, De Rosa et al. 2004, Zdziarski et al. 2003). In summary, in the broad X-ray range from 0.1 to 200 keV, NGC 4151 represents a case study of the common properties (absorption/scattering medium) of type 1 and type 2 objects, of AGN environment from light-day to kpc, and of investigation of the properties of the intrinsic continuum.

In this paper we present the results of the complete set of observations by *BeppoSAX* performed in 1996, 1999, 2000 and 2001. The observations and data reduction are described in Section 2. A model-independent variability study is presented in Section 3. The broad-band spectral analysis is reported in Section 4 and discussed in Section 5. Our conclusions are drawn in Section 6.

2. *BeppoSAX* observations and data reduction

NGC 4151 was observed by *BeppoSAX* (Piro, Scarsi & Butler 1995; Boella et al. 1997) several times: in July 1996, December 1996, January 1999, December 2000 and December 2001. The log of the observations is given in Table 1.

The first observation, part of the Science Verification Phase (SVP), was originally planned to last for about 3 days. However the pointing was interrupted for 1 day and then restarted 2 days after. In the observations in 1996 the three MECS units, the HPGSPC and the PDS were operated. The LECS was always on, with the exception of the second part of the observation in July 1996. From January 1999 onward two MECS units, the LECS and the PDS were operating.

The data of all instruments were reduced using standard procedures (Fiore, Guainazzi & Grandi 1999). A BL Lac object is located $\sim 5'$ away from NGC 4151. The count rates are ~ 2 per cent and ~ 20 per cent of that of NGC 4151 for the MECS and LECS respectively. For the

MECS we adopted the standard extraction circle of $4'$, in which the contribution of the BL Lac is negligible ($\lesssim 0.4$ per cent). In the extraction of spectra and light curves of LECS we excluded a circle of $2'$ of radius centered on the BL Lac object, while adopting the standard source extraction radius of $8'$. We estimate a residual contribution of the BL Lac of $\approx 5 - 10$ per cent, comparable to the statistical errors. The PDS spectra filtered either with fixed or variable rise time thresholds did not show any significant difference. The latter method is more suited to sources fainter than NGC 4151, so we have adopted data derived with the first method.

In Figure 1 we show the light curves of the LECS (0.1–2 keV), MECS (2–10 keV) and PDS (13–100 keV). The MECS (2–10 keV) counts rate during the July 1996 observation changed by a factor of two on time scales of one day, from a low state (hereafter J96L) to a high state (J96H). The intensity during the December 1996 observation was constant (D96), and quite similar to the J96L state, then low. Also the observation in December 2000 (D00) was constant. In January 1999 the average flux was at an intermediate level between the Low and High states defined above. During the observation the source flux exhibited a slow increase in the first part of the observation (J99L1), reached a peak (J99H) and then started to decrease (J99L2). The time scale was ~ 0.5 days, with an amplitude of ~ 1.8 (max to min). The PDS (13–100 keV) light curve follows the same pattern of variability of the MECS, but with a reduced amplitude: for example the ratio high to low states in July 1996 is 2.00 ± 0.01 for the MECS and 1.22 ± 0.03 for the PDS (Table 1). On the reverse the LECS (0.1–2 keV) count rate, with the exception of December 2001 (D01), does not show significant variability: the small difference (< 20 per cent, see Table 1) of level between different observations is consistent with the effect of grid obscuration of the source (Fiore, Guainazzi & Grandi 1999), placed in different positions in the three observations. The different behaviour in December 2001 will be discussed in Section 4.6. Considering the substantial amount of spectral variability shown by this object, we have produced separate spectra for each of the above mentioned states, in which (2–10 keV) variations are $\lesssim 25$ per cent.

Hereafter errors and upper limits on spectral parameters correspond to $\Delta\chi^2 = 2.7$, i.e. 90 per cent confidence level for a single parameter of interest. Spectral power indexes refer to photon distribution. In spectral fitting the normalizations of LECS, HPGSPC and PDS relative to the MECS have been left free to vary within the current ranges of uncertainty: LECS/MECS: 0.7–1.0; HPGSPC/MECS=0.95–1.1; PDS/MECS=0.77–0.95.

3. Spectral ratios

The spectral ratios derived comparing the spectral states observed during our campaign are presented in Figure 2.

Table 1. Log of the observations

Date	LECS (0.1–2 keV)		MECS (2–10 keV)		HPGSPC (8–20 keV)		PDS (13–200 keV)	
	t_{exp}^1	cnt rate ²	t_{exp}^1	cnt rate ²	t_{exp}^1	cnt rate ²	t_{exp}^1	cnt rate ⁵
6-10/7/96 (J96L)	6	0.065 ± 0.003	56	1.145 ± 0.005^3	26	1.86 ± 0.06	26	2.36 ± 0.02
“ (J96H)	-	-	15	2.29 ± 0.01^3	7	2.7 ± 0.1	8	2.90 ± 0.04
4-7/12/96 (D96)	13	0.051 ± 0.003	48	1.102 ± 0.005^3	23	1.9 ± 0.06	19	2.28 ± 0.03
4-6/1/99 (J99L1)	14	0.053 ± 0.002	36	0.937 ± 0.005^4	-	-	16	2.55 ± 0.04
“ (J99H)	10	0.057 ± 0.003	27	1.238 ± 0.007^4	-	-	13	2.95 ± 0.04
“ (J99L2)	10	0.059 ± 0.002	20	1.015 ± 0.007^4	-	-	9	2.60 ± 0.04
22-23/12/2000 (D00)	4	0.035 ± 0.003	19	0.470 ± 0.005^4	-	-	9	1.01 ± 0.04
18-21/12/2001 (D01)	43	0.145 ± 0.002	114	1.929 ± 0.004^4	-	-	53	2.90 ± 0.01

Note: ¹ net exp. time in ks; ² s⁻¹. For the MECS we indicate the total rate of all MECS unit operating; ³ 3 MECS units; ⁴ 2 MECS units; ⁵ s⁻¹ per half detector

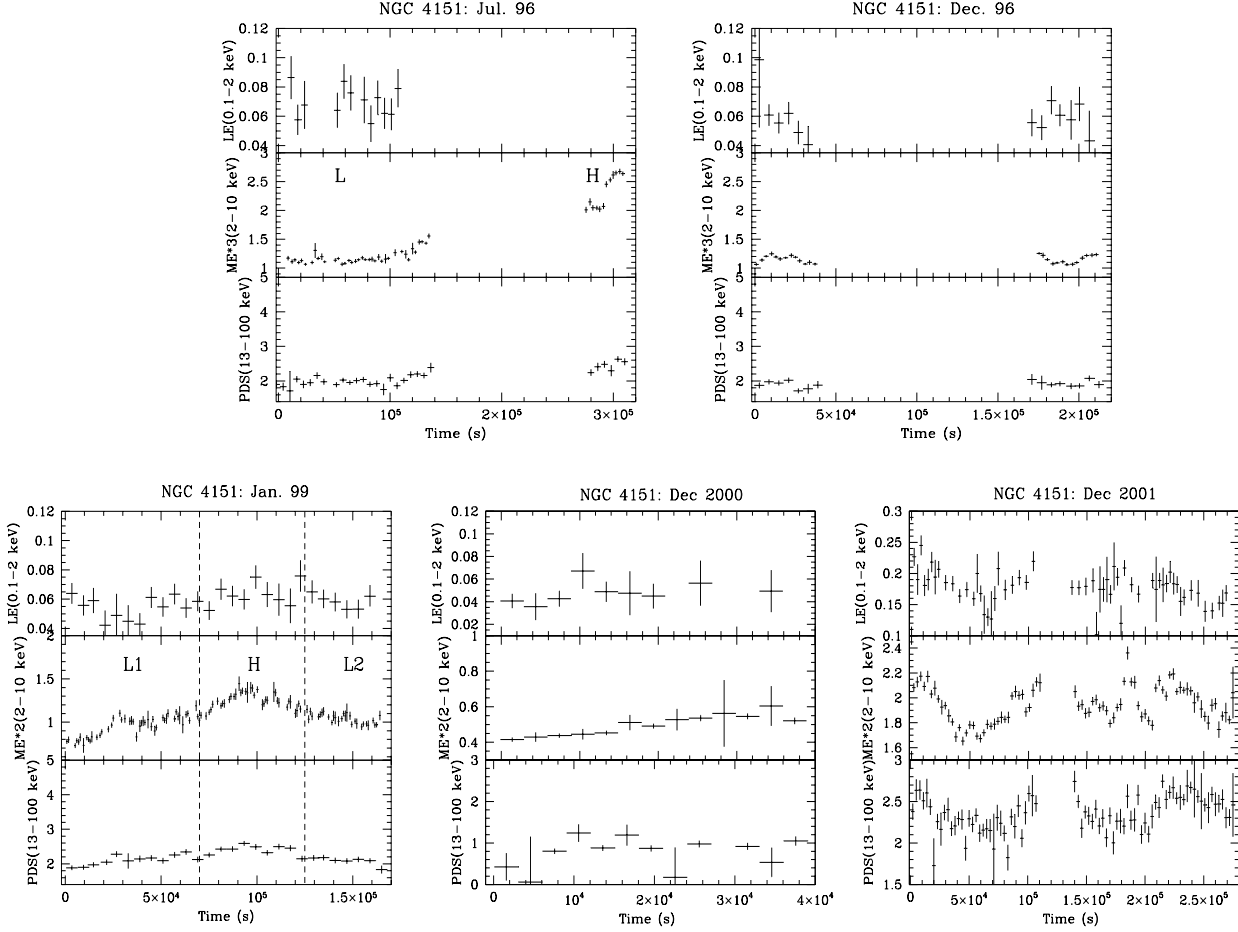


Fig. 1. Light curve of NGC4151 in cts/s. We note that from 1999 onward (lower panels) two MECS units were operating, while in 1996 (upper panels) they were three.

This allows us to derive a model-independent description on the spectral variability of the source. We note the following:

1. Below 1 keV the flux remains constant, notwithstanding the large variations showed at $E \gtrsim 2$ keV. The low energy spectrum is thus to be dominated by constant component(s) (Perola et al. 1986; Pounds et al. 1986; Zdziarski et al. 1996). This means that some absorber has to suppress any variable intrinsic component at low energies. Around 0.6–0.7 keV the ratio D01/D00 shows evidence of a changing of the opacities of the warm gas. We will discuss this effect in Section 4.2.
2. The 2–10 keV range is characterized by the largest variability, up to a factor of ~ 8 in the 2–3 keV range. The spectrum gets steeper when the flux increases (J96H/J96L, J99H/J99L1, D01/D00, J99H/J96L). This happens both on short (days) and long time scales (years). This behaviour has been attributed to intrinsic spectral variations correlated with the luminosity on time scale as short as few hours (Yaqoob et al. 1993; Perola et al. 1986), and to variations of the absorber on month-year time scales. Warwick et al. (1995) and

Weaver et al. (1994b) instead attributed all variations to changes of absorber structure. We will assess this issue through a broad band spectral fitting (see Section 4.1).

3. Above 10 keV two kind of behaviour are apparent. a) The spectral ratios relative to observations performed within \approx day are all consistent with a constant (J96H/J96L: $\chi^2_\nu = 1.2$, J99L2/J99L1: $\chi^2_\nu = 0.6$ and J99H/J99L1: $\chi^2_\nu = 1.2$). b) The spectral ratios relative to observations performed over time scales of months-years are not (J96H/J99H: $\chi^2_\nu = 2.0$, and D01/D00: $\chi^2_\nu = 1.8$, and J99H/J96L: $\chi^2_\nu = 2.6$). This is a new result that, as it will be shown in Section 4.3, bears important implications on the origin of the reflection component.

In the next sections we will present a detailed quantitative analysis of these results, through detailed spectral deconvolution.

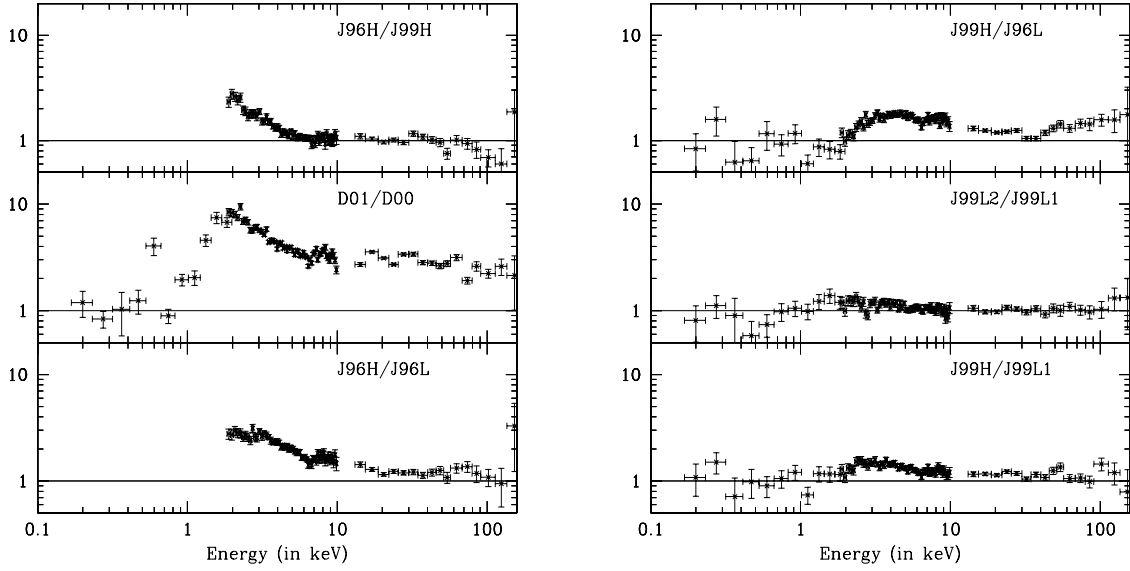


Fig. 2. Spectral ratio between different states.

4. Broad-band (0.1–200 keV) spectral modelling

On the basis of previous observations and models developed in previous published work, to fit the *BeppoSAX* broad-band spectra (with all the instruments in the energy range specified in Table 1), we adopted a spectral template model (*baseline model* BLM), which includes the following components:

A. The intrinsic continuum is described by a power-law with an e-folding energy E_c .

B. A Compton reflection component (PEXRAV model in XSPEC, Magdziarz & Zdziarski 1995), with the cosine of inclination angle of the reflector fixed to 0.95. We assume elemental abundances from Anders & Grevesse (1989).

C. A narrow $K\alpha$ iron line modeled with a gaussian profile with the intrinsic width set to 10 eV.

D. The soft X-ray spectrum ($E < 2$ keV) is a combination of a thermal component model (MEKAL) with the temperature fixed to 0.15 keV and a scattering component (i.e. a power-law with the same slope of the intrinsic hard continuum but with a different normalization).

E. The complex absorber is reproduced with a dual absorber model. A fraction f_{cov} of the source is covered by a cold column density N_{Hcov} . An additional uniform and photoionized gas is responsible for additional absorption of the spectrum at low energies and for a midly ionized Fe edge at 7.3–7.5 keV (FeVII-FeVIII) (ABSORI model in XSPEC Done et al. 1992).

This photoionized gas is characterized by a temperature $T = 3 \times 10^4$ K, a column density N_{Hwarm} and a ionization parameter $\xi = L_{\text{ion}}/nR^2$, where L_{ion} is the source luminosity between 5 eV and 300 keV, n is the hydrogen number density of the gas and R its distance from the cen-

tral ionizing source. The Fe abundances in the cold and warm absorbers and in the reflection component are tied together and left free during the fit.

Our model assumes that only the e-folded power-law with reflection (i.e. the intrinsic continuum), is subject to complex absorption. Additional absorption through the Galaxy is applied to *all* the emission components ($N_{\text{Hgal}} = 2 \times 10^{20} \text{ cm}^{-2}$).

The BLM model is shown in Figure 3. In the upper panel in Figure the spectrum with model of J96L is plotted with all the different spectral components while in the lower panel two spectral states with a flux variation of a factor of ~ 3 (see Table 2) are shown: December 2000 and December 2001. We applied this template to all the *BeppoSAX* spectra in the different flux level states (see Table 1 and light curves in Figure 1). The best fit parameters and the reduced χ^2 values are shown in Table 2, while the data/model ratio for each spectrum is plotted in Figure 4. In the case of July 1996 high state (when LECS data are not available) the parameters of the soft components (thermal emission and scattering component) are frozen to those derived for the spectrum in July 1996 low state.

The broad-band baseline model described above provides a good fit to all the spectra of NGC 4151 (Table 2). In the following sections we discuss the various spectral components and their variability.

4.1. The origin of the spectral variability in the 2–10 keV range and the intrinsic power law

The source has always shown - in all the observations performed so far and including ours - a systematic trend: the spectrum gets softer when the flux increases. The origin of this behaviour is one of the key issue in this source.

Table 2. Broad band (1.8-200 keV) fits with our BLM. E_C is the e-folding energy of the intrinsic continuum, A_{IC} the normalization of the intrinsic continuum at 1 keV, A_{refl} is the strength of the Compton reflection hump obtained as $\Omega/2\pi \times A_{IC}$, I_{Fe} is the flux of the iron line at 6.4 keV, N_{Hcov} and N_{Hwarm} are the column densities of the cold partially covered and warm gas respectively, f_{cov} is the covered fraction of the cold gas, ξ is the ionization parameter of the warm gas, EM_{thermal} is the emission measure of the thermal gas - defined by $\int n_e n_H dV$, where n_e is the electron density, and n_H is the hydrogen density - assuming the distance to the source of 13 Mpc, and A_{scatt} is the 1 keV flux of soft scattered component.

Period	Γ	$^1 E_C$	$^2 A_{IC}$	$^2 A_{\text{refl}}$	$^3 I_{\text{Fe}}$	$(Z/Z_{\odot})_{\text{Fe}}$	$^4 N_{\text{Hcov}}$	f_{cov}	$^4 N_{\text{Hwarm}}$	$^5 \xi$	$^7 EM_{\text{therm}}$	$^8 A_{\text{scatt}}$	$^6 F_{2-10\text{keV}}^{\text{unabs}}$	$^6 F_{0.1-200\text{keV}}^{\text{unabs}}$	χ^2_{ν}
J96L	$1.58^{+0.37}_{-0.39}$	143^{+380}_{-84}	$3.9^{+2.9}_{-2.0}$	$2.4^{+4.2}_{-2.5}$	$4.0^{+0.7}_{-0.5}$	$1.4^{+2.3}_{-0.5}$	$22.1^{+5.1}_{-8.3}$	$0.68^{+0.05}_{-0.08}$	$5.4^{+1.8}_{-1.8}$	8*	$7.0^{+9.1}_{-7.0}$	$2.1^{+0.7}_{-0.5}$	2.04	10.5	96
J96H	$1.51^{+0.05}_{-0.22}$	81^{+40}_{-20}	$5.4^{+2.6}_{-1.4}$	$1.0^{+0.6}_{-1.0}$	$2.7^{+1.0}_{-1.0}$	$1.8^{+0.7}_{-0.5}$	$11.0^{+7.8}_{-3.7}$	$0.49^{+0.25}_{-0.14}$	$2.1^{+1.0}_{-2.0}$	16*			3.01	13	76
D96	$1.63^{+0.22}_{-0.27}$	130^{+221}_{-58}	$4.1^{+2.1}_{-0.5}$	$2.1^{+2.3}_{-1.3}$	$4.1^{+0.5}_{-0.5}$	$1.5^{+0.3}_{-0.3}$	$22.0^{+12.2}_{-5.2}$	$0.57^{+0.04}_{-0.07}$	$9.4^{+2.8}_{-2.2}$	9.3*	$8.6^{+7.4}_{-6.7}$	$2.2^{+0.6}_{-0.4}$	2.01	11	64
J99L1	$1.59^{+0.18}_{-0.17}$	125^{+129}_{-32}	$5.5^{+2.3}_{-1.7}$	$0.27^{+1.2}_{-0.27}$	$4.2^{+0.8}_{-0.8}$	$1.7^{+0.6}_{-0.4}$	$21.0^{+6.3}_{-5.3}$	$0.64^{+0.07}_{-0.09}$	$8.5^{+1.6}_{-2.0}$	8.5*	$12.4^{+7.3}_{-5.5}$	$1.8^{+0.5}_{-0.4}$	2.72	13	61
J99H	$1.74^{+0.22}_{-0.24}$	177^{+2473}_{-83}	$8.1^{+4.6}_{-2.9}$	$1.3^{+1.6}_{-1.3}$	$2.8^{+0.9}_{-0.9}$	$1.6^{+1.1}_{-0.6}$	$19.8^{+5.6}_{-6.4}$	$0.58^{+0.07}_{-0.08}$	$6.8^{+1.4}_{-1.4}$	2.9*	$14.3^{+7.3}_{-5.5}$	$2.5^{+0.8}_{-0.7}$	3.38	16.5	85
J99L2	$1.56^{+0.27}_{-0.21}$	130^{+496}_{-53}	$4.6^{+2.2}_{-1.7}$	$0.6^{+2.0}_{-0.6}$	$4.2^{+1.0}_{-0.9}$	$1.8^{+0.6}_{-0.9}$	$12.3^{+5.4}_{-5.4}$	$0.70^{+0.12}_{-0.32}$	$6.4^{+3.7}_{-2.0}$	10.3*	$3.5^{+6.7}_{-3.5}$	$2.0^{+0.7}_{-0.5}$	2.44	13	73
D00	$1.71^{+0.17}_{-0.23}$	> 200	$2.4^{+2.8}_{-1.1}$	$1.3^{+2.0}_{-1.3}$	$2.1^{+1.4}_{-0.7}$	$1.7^{+1.7}_{-1.1}$	30^{+94}_{-24}	$0.34^{+0.21}_{-0.24}$	$8.3^{+3.9}_{-4.2}$	7.8*	$3.0^{+12.1}_{-3.0}$	$1.5^{+0.6}_{-0.4}$	1.01	5.9	71
D01	$1.52^{+0.02}_{-0.06}$	122^{+13}_{-11}	$4.7^{+0.3}_{-0.3}$	$0.03^{+0.25}_{-0.03}$	$2.8^{+0.4}_{-0.4}$	$5.8^{+1.0}_{-2.1}$	$3.5^{+1.1}_{-0.9}$	$0.39^{+0.08}_{-0.07}$	$0.9^{+0.2}_{-0.3}$	0.7*	$4.2^{+6.5}_{-4.2}$	$2.5^{+0.8}_{-0.7}$	2.66	14	71

Note: ⁽¹⁾ e-folding energy in keV; ⁽²⁾ in $10^{-2} \text{ keV}^{-1} \text{ cm}^{-2} \text{ s}^{-1}$; ⁽³⁾ in $10^{-4} \text{ cm}^{-2} \text{ s}^{-1}$ at the line; ⁽⁴⁾ in 10^{22} cm^{-2} ; ⁽⁵⁾ in erg cm s^{-1} ; ⁽⁶⁾ in $10^{-10} \text{ erg cm}^{-2} \text{ s}^{-1}$; ⁽⁷⁾ in 10^{62} cm^{-3} ; ⁽⁸⁾ in $10^{-3} \text{ keV}^{-1} \text{ cm}^{-2} \text{ s}^{-1}$; * These parameters are frozen to their values of best fit computing the errors.

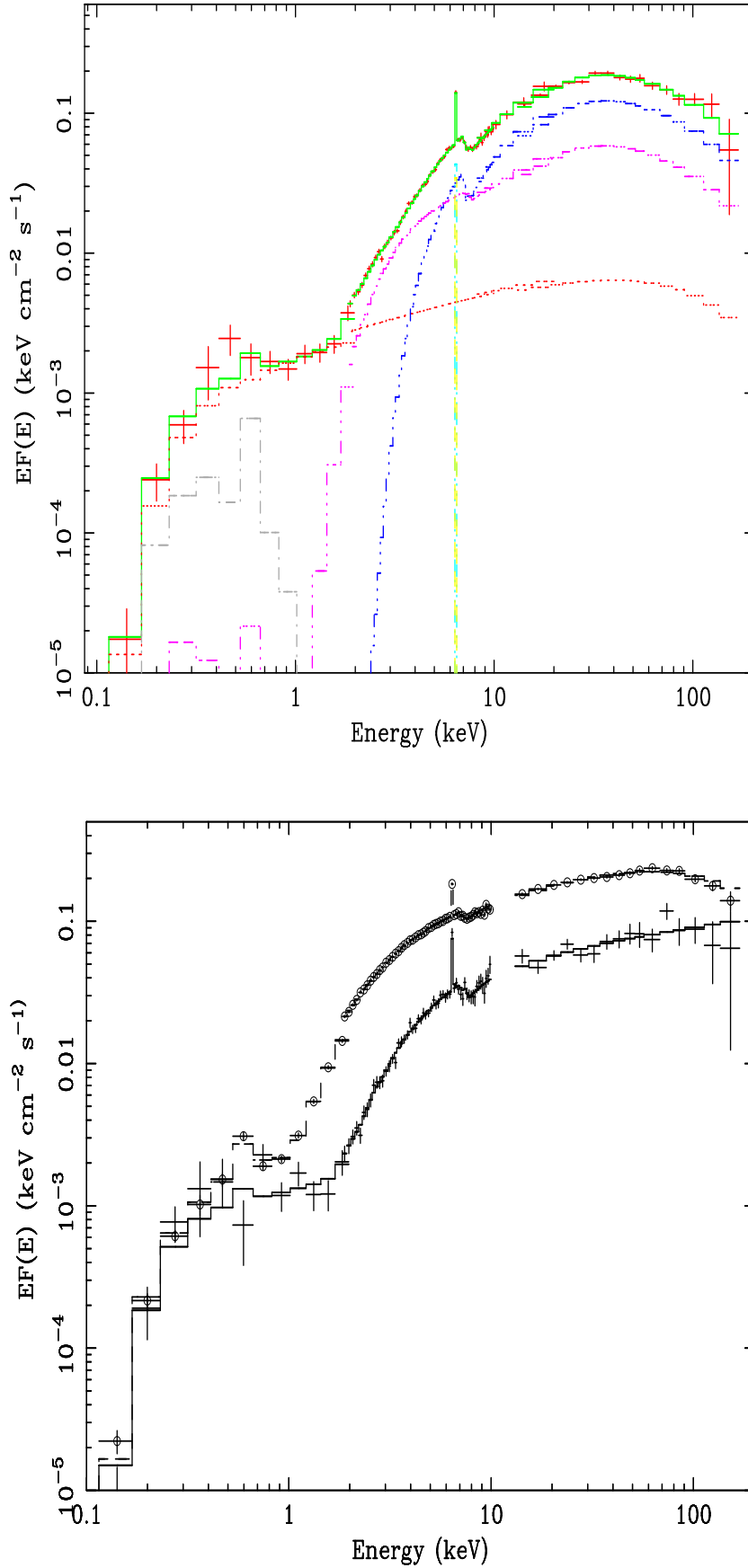


Fig. 3. *BeppoSAX* broad-band spectrum $EF(E)$. In the upper panel we plot the spectrum in July 1996 low state with all the spectral components of the BLM described in the text: in green (solid line) the total spectrum, in red (dot line) the scattered component, in grey (dash-dot line) the thermal soft component, in blue and magenta (dash-dot-dot lines) the transmitted components

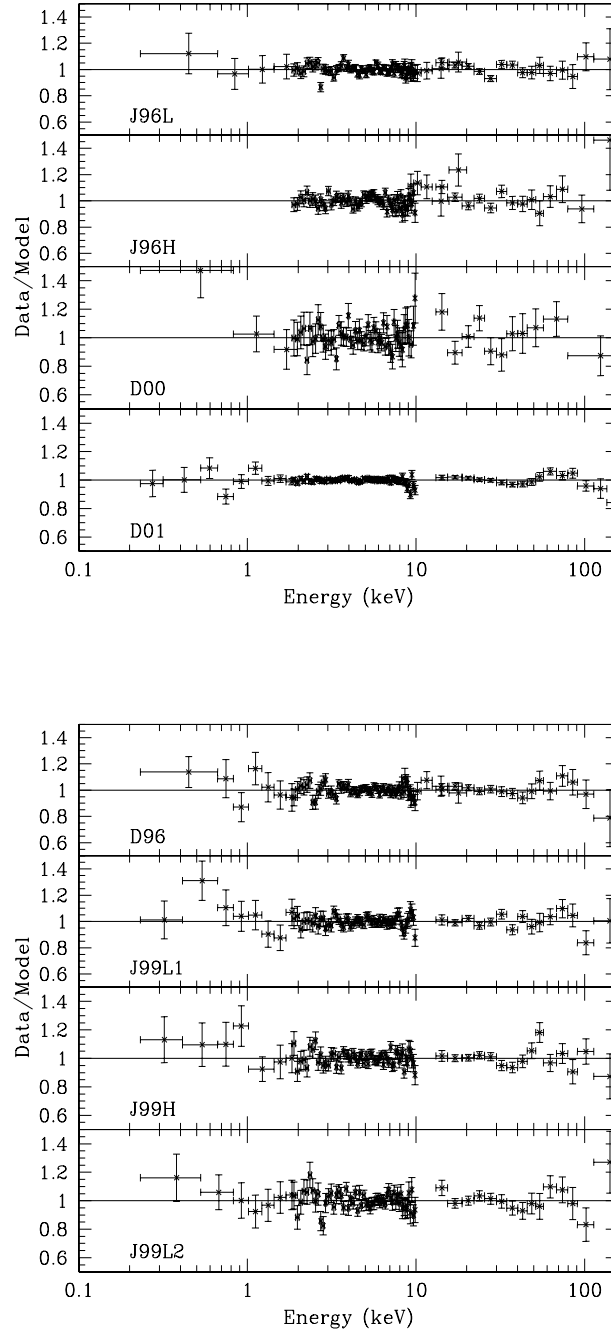


Fig. 4. The Data/model ratios for the baseline model.

The broad band fit (presented in Table 2) shows that which can be related to the 2–10 keV spectral variability, the only spectral parameters showing significant changes,

are those of the absorbing media. Indeed, a decrement of the effective absorption (i.e. of N_{H} and/or f_{cov}) results in a softer spectrum, as appears when comparing the spectral ratios presented in Section 3 with the best fit parameters in Table 2. For example, the softening observed from J96L to J96H (Figure 2) is reproduced by decreasing the column densities of the two absorbers and the covering fraction (Table 2). On the contrary the intrinsic photon index does not show significant evidence of variation around the average value of $\Gamma \approx 1.6$. A variation $\Delta\Gamma \approx 0.2$ would still be consistent with the errors, but it could not itself account for the large spectral changes observed in this range. While most of the spectral variability observed in the 2–10 keV range is due to variation of the absorbers, a minor effect of intrinsic variations can not be excluded. This is demonstrated by fitting the spectra with the intrinsic photon index given by the $F_{2-10\text{keV}}$ vs Γ relation found by Perola et al. (1986): $\Gamma = 2.18 + 0.012 \times F_{2-10\text{keV}}$ with $F_{2-10\text{keV}}$ in 10^{-11} erg cm $^{-2}$ s $^{-1}$. The results of these fits are reported in Table 3 and show that in all spectra a good χ^2_{ν} is obtained.

4.2. The complex absorber

With the exception of the 2001 observation, the cold absorber is characterized by $N_{\text{Hcov}} = (1 - 3) \times 10^{23}$ cm $^{-2}$ and $f_{\text{cov}} = 0.3 - 0.7$, similar to that found by Weaver et al. (1994b), who adopted the same model of this analysis on *ASCA* data. The model employed for the warm gas with $\xi \sim 1\text{--}16$ erg cm s $^{-1}$ indicates an iron edge at energy around 7.3–7.6 keV, consistently with other measurements (Yaqoob et al. 1993; Weaver et al. 1994a; Weaver et al. 1994b; Schurch et al. 2003). With the exception of D01, the iron abundance is ≈ 1.5 times greater than the solar value. We will show later how D01 is peculiar in respect to several points.

With regard to the variability of absorbers, we note the following. Due to the fit with such a complex model, the errors on the absorbers parameters are wide. However we note that the column density of the warm absorber appears to show the most significant variations in respect to those of the cold absorber. We have therefore chosen to fix the column density of the cold absorber to the average value $N_{\text{Hcov}} = 15 \times 10^{22}$ cm $^{-2}$. This is consistent, within the errors, with all the best fit values except D01. In addition we have fixed the spectral index, as from the above discussion, to the value 1.6. The result and all the best fit parameters are reported in Table 4. The χ^2 is still acceptable. The column density of the warm absorber changes over a time scale of month-years, while it is consistent with being constant over a day time scale. Specifically, in July 1996, $N_{\text{Hwarm}} \approx 3.5 \times 10^{22}$ cm $^{-2}$, in D96 to D00 $N_{\text{Hwarm}} \approx 7 \times 10^{22}$ cm $^{-2}$. On the contrary the covering fraction of the cold absorber shows variability in a day time scale. For example changing from 0.73 to 0.48 in the low and high state of July 1996.

The D01 spectrum appears to be rather peculiar with respect to the other states. We already noted that in this state the iron abundance is about 5 times that solar. In D01 the softening is reproduced with a substantial decrease of the thickness of both absorbers, with $N_{\text{Hcov}} = 3.5 \times 10^{22}$ cm $^{-2}$, $N_{\text{Hwarm}} = 0.9 \times 10^{22}$ cm $^{-2}$. The covering fraction was also very low, $f_{\text{cov}} \approx 0.3$. Basically, in the state observed by *BeppoSAX* in December 2001, most of the bare nuclear continuum came into view (Figure 3, lower panel). The D01 spectrum is peculiar also for the presence of an absorption feature at ~ 9 keV. This state of the source is described and discussed in Piro et al. (2005).

4.3. The reflection component

The Compton reflection component is significantly detected in 1996 (both in July and December, with a mean value of the *absolute* normalization $A_{\text{reff}} = (2.2 \pm 0.3) \times 10^{-2}$ ph cm $^{-2}$ s $^{-1}$ keV $^{-1}$), it is only marginally detected in 1999 ($A_{\text{reff}} = (0.8 \pm 0.3) \times 10^{-2}$ ph cm $^{-2}$ s $^{-1}$ keV $^{-1}$), while it is consistent with zero in 2000 and 2001 (see Table 4). This result remains true even when the photon index is not fixed (see Table 2 and Table 3). Thus we find that the reflection component is variable on time scales of years, while there is not strong evidence of variability on the (intra) day time scales that characterize the direct continuum. We can actually exclude variations correlated with those of the intrinsic continuum on such short time scales.

4.4. High-energy spectral variability

In Section 4.2 we have concluded that the spectral variability observed in the 2–10 keV range is dominated by variations of the absorber. At higher energies, although the effect of absorption is negligible, the assessment is also not straightforward due to the presence of the reflection component. For example, a *constant* absolute reflection component, added to a steep (constant slope) variable continuum (Schurch & Warwick 2002), may also qualitatively mimic the Γ vs $F_{2-10\text{keV}}$ correlation. It is then particularly relevant to discuss the high energy spectra in 2000 and 2001 when the reflection intensity is consistent with zero and then any intrinsic spectral variation can be observed without ambiguity. Between 10 keV and 200 keV the spectral ratio D01/D00 is not consistent with a constant ($\chi^2_{\nu} = 1.8$ per 15 degree of freedom), but shows a decreasing trend that can be reproduced with a change of the intrinsic slope between the two states of about 0.17 ± 0.06 (with the assumption of a constant high energy cut-off). This result is that expected on the basis of the correlation Γ vs $F_{2-10\text{keV}}$, where $F_{2-10\text{keV}}$ is changing by a factor of three between D00 and D01.

Table 3. As Table 2 with the intrinsic photon index Γ frozen following the $F_{2-10\text{keV}}$ vs Γ relation found by Perola et al. 1986.

Period	Γ	1E_c	$^2A_{\text{IC}}$	$^2A_{\text{refl}}$	$^3I_{\text{Fe}}$	$(Z/Z_{\odot})_{\text{Fe}}$	$^4N_{\text{Hcov}}$	f_{cov}	$^4N_{\text{Hwarm}}$	$^5\xi$	$^7EM_{\text{therm}}$	$^8A_{\text{scatt}}$	$^6F_{2-10\text{keV}}^{\text{unabs}}$	χ^2_{ν}
J96L	1.42	68 ± 5	$3.0^{+0.2}_{-0.2}$	$1.1^{+0.4}_{-0.4}$	$3.9^{+0.5}_{-0.5}$	$2.3^{+0.4}_{-0.3}$	$20.1^{+4.3}_{-2.7}$	$0.66^{+0.04}_{-0.06}$	$5.1^{+1.7}_{-1.1}$	10*	$8.1^{+7.6}_{-5.7}$	$2.2^{+0.6}_{-0.5}$	2.04	96.4/78
J96H	1.54	86^{+11}_{-11}	$5.2^{+0.7}_{-0.5}$	$1.6^{+0.9}_{-0.9}$	$2.9^{+0.9}_{-0.9}$	$2.9^{+1.4}_{-1.1}$	$10.4^{+6.2}_{-7.3}$	$0.50^{+0.18}_{-0.09}$	$2.6^{+0.8}_{-1.1}$	16*			3.01	73.2/68
D96	1.42	79^{+10}_{-10}	$2.8^{+0.3}_{-0.2}$	$1.0^{+0.4}_{-0.4}$	$4.1^{+0.5}_{-0.5}$	$2.0^{+0.4}_{-0.4}$	$18.1^{+10.1}_{-4.5}$	$0.54^{+0.10}_{-0.13}$	$8.3^{+2.2}_{-1.8}$	8.3*	$10.0^{+5.2}_{-4.7}$	$2.0^{+0.3}_{-0.3}$	2.01	65.6/78
J99L1	1.51	100^{+10}_{-10}	$4.6^{+0.4}_{-0.2}$	> 0.5	$4.2^{+0.7}_{-0.8}$	$1.8^{+0.4}_{-0.3}$	$19.6^{+5.5}_{-2.4}$	$0.63^{+0.07}_{-0.08}$	$7.9^{+0.9}_{-2.5}$	8.7*	$13.0^{+6.1}_{-7.0}$	$1.8^{+0.4}_{-0.4}$	2.72	61.9/73
J99H	1.59	122^{+15}_{-13}	$6.5^{+0.5}_{-0.4}$	$0.3^{+0.6}_{-0.3}$	$2.9^{+0.9}_{-0.9}$	$2.1^{+0.5}_{-0.4}$	$17.3^{+4.9}_{-3.3}$	$0.56^{+0.06}_{-0.07}$	$6.3^{+1.1}_{-0.9}$	2.7*	$14.4^{+7.5}_{-5.4}$	$1.5^{+0.5}_{-0.4}$	3.38	86.2/73
J99L2	1.47	100^{+14}_{-11}	$3.9^{+0.3}_{-0.3}$	$0.2^{+0.6}_{-0.2}$	$4.2^{+0.9}_{-0.9}$	$2.1^{+0.7}_{-0.6}$	$10.9^{+6.2}_{-2.6}$	$0.67^{+0.15}_{-0.28}$	$6.5^{+3.8}_{-2.0}$	10.9*	$5.1^{+6.5}_{-5.1}$	$2.0^{+0.7}_{-0.5}$	2.44	73.1/73
D00	1.30	110^{+25}_{-25}	$1.0^{+0.1}_{-0.1}$	< 0.1	$1.9^{+0.5}_{-0.5}$	8^{+11}_{-5}	$2.1^{+1.6}_{-1.3}$	$1.0^{+0.0}_{-0.6}$	$1.6^{+3.3}_{-1.4}$	10*	$2.3^{+4.4}_{-1.6}$	$1.3^{+0.3}_{-0.3}$	1.01	74.8/73
D01	1.50	122^{+7}_{-5}	$4.7^{+0.1}_{-0.1}$	< 0.2	$2.8^{+0.4}_{-0.4}$	$7.1^{+2.2}_{-2.1}$	$3.1^{+0.9}_{-0.6}$	$0.41^{+0.09}_{-0.07}$	$0.8^{+0.2}_{-0.2}$	0.3*	$2.8^{+2.3}_{-1.2}$	$2.3^{+0.5}_{-0.9}$	2.66	70.3/73

Note: ⁽¹⁾ e-folding energy in keV; ⁽²⁾ in 10^{-2} keV $^{-1}$ cm $^{-2}$ s $^{-1}$; ⁽³⁾ in 10^{-4} cm $^{-2}$ s $^{-1}$ at the line; ⁽⁴⁾ in 10^{22} cm $^{-2}$; ⁽⁵⁾ in erg cm s $^{-1}$; ⁽⁶⁾ in 10^{-10} erg cm $^{-2}$ s $^{-1}$; ⁽⁷⁾ in 10^{62} cm $^{-3}$; ⁽⁸⁾ in 10^{-3} keV $^{-1}$ cm $^{-2}$ s $^{-1}$; * These parameters are frozen to their values of best fit computing the errors.

Table 4. As Table 2, without less important component, with $\Gamma=1.6$ and the cold column density $N_{\text{Hcov}} = 15 \times 10^{22} \text{cm}^{-2}$.

Period	¹ E_c	² A_{IC}	² A_{refl}	³ I_{Fe}	f_{cov}	⁴ N_{Hwarm}	⁵ ξ	χ^2_ν
J96L	106^{+10}_{-10}	$3.3^{+0.2}_{-0.1}$	$3.3^{+0.6}_{-0.3}$	$4.2^{+0.4}_{-0.4}$	$0.73^{+0.03}_{-0.04}$	$4.4^{+1.4}_{-0.9}$	8*	104/79
J96H	98^{+14}_{-11}	$6.6^{+0.7}_{-0.8}$	$1.2^{+0.6}_{-0.6}$	$3.4^{+1.1}_{-0.5}$	$0.48^{+0.05}_{-0.09}$	$3.1^{+1.9}_{-0.8}$	16*	73/69
D96	124^{+15}_{-15}	$3.5^{+0.2}_{-0.2}$	$2.2^{+0.5}_{-0.3}$	$4.1^{+0.5}_{-0.4}$	$0.60^{+0.10}_{-0.08}$	$8.0^{+2.1}_{-1.5}$	9.9*	76/79
J99L1	135^{+18}_{-15}	$5.0^{+0.3}_{-0.3}$	$1.0^{+0.4}_{-0.4}$	$4.2^{+0.7}_{-0.7}$	$0.73^{+0.04}_{-0.06}$	$6.9^{+1.6}_{-1.2}$	8.6*	73/74
J99H	127^{+16}_{-14}	$6.0^{+1.0}_{-0.7}$	$0.6^{+0.5}_{-0.5}$	$2.9^{+0.9}_{-0.9}$	$0.60^{+0.04}_{-0.05}$	$6.0^{+1.0}_{-0.7}$	3.2*	87/74
J99L2	144^{+30}_{-20}	$5.1^{+0.4}_{-0.4}$	$0.8^{+0.6}_{-0.5}$	$4.2^{+0.9}_{-0.9}$	$0.73^{+0.07}_{-0.16}$	$7.4^{+3.0}_{-1.5}$	9.7*	74/74
D00	422^{+3965}_{-225}	$1.8^{+0.1}_{-0.3}$	< 0.5	$2.0^{+0.5}_{-0.6}$	$0.34^{+0.14}_{-0.28}$	$6.7^{+3.1}_{-1.7}$	14*	71/74
D01	162^{+12}_{-11}	$6.0^{+0.2}_{-0.2}$	$0.3^{+0.3}_{-0.2}$	$2.6^{+0.5}_{-0.4}$	$0.28^{+0.02}_{-0.03}$	$1.9^{+0.2}_{-0.1}$	2.8*	107/74

Note: ⁽¹⁾ keV; ⁽²⁾ in $10^{-2} \text{keV}^{-1} \text{cm}^{-2} \text{s}^{-1}$; ⁽³⁾ in $10^{-4} \text{cm}^{-2} \text{s}^{-1}$ at the line; ⁽⁴⁾ in 10^{22}cm^{-2}

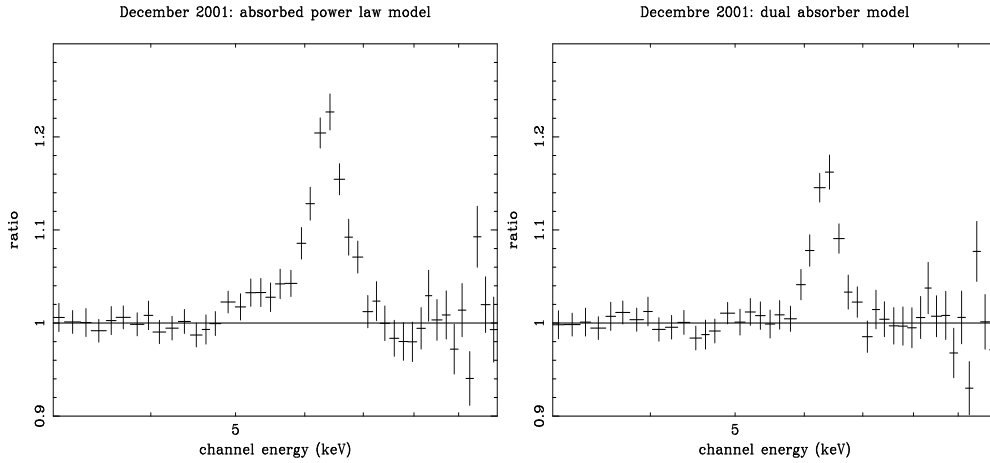


Fig. 5. In the left panel we show the iron line profile when the continuum is reproduced with a simple absorbed power law in 3-10 keV. Clear positive residuals are evident between 5-6 keV. When the continuum is correctly modeled with a dual absorber model (our BLM), the residuals disappear, on the right panel, and a narrow gaussian profile becomes a good description to the iron line. The broadening of the profile in right panel is due to the MECS resolution (8 per cent at 6 keV).

4.5. The iron line

We recall that, in our modelling, we have adopted a narrow gaussian profile for the line without any further component, following the results of *Chandra* and *XMM-Newton* (Ogle et al. 2000; Schurch et al. 2003). Because the issue of the existence and origin of broad components in Seyfert galaxies is still under debate, it is relevant to underline how this is dependent upon a good modelling of the continuum, available thanks to the *BeppoSAX* broad-band data. In Figure 5 we show the residuals when the continuum is modelled by a simple uniform absorbed power law and the line shows evidence of a “red wing”. However, when the continuum is properly described with a dual absorber, the “red wing” – which is in fact due to the covered component – disappears.

The flux of the iron line in our spectra shows evidence of variability ($\chi^2/dof = 19.6/7$ for a constant, chance probability $P=0.0065$), but these variations are not correlated with the intensity of the intrinsic continuum (cor-

relation coefficient $r=0.099$). Interestingly the flux of the line is lower in D00 and D01 when the reflection component disappears. To explore this issue we plot in Figure 6 the line *vs* reflection intensity. A linear fit, plotted in the figure, is acceptable ($\chi^2/dof = 7.8/6$, $P=0.253$) with $I = (2.5 \pm 0.3) \times 10^{-4} + (0.57 \pm 0.17) \times 10^{-2} A_{\text{refl}}$, I is in $\text{ph cm}^{-2} \text{s}^{-1}$ and A_{refl} in $\text{ph cm}^{-2} \text{s}^{-1} \text{keV}^{-1}$. This fit shows that when the reflection component is null, the line flux does not go to zero, identifying the presence of a constant line component in addition to the one that correlates with the reflection. While it is not statistically significant, it is nonetheless interesting to note that for large value of the reflection normalization, the line appears to saturate. This point will be discussed later.

4.6. The soft components

In the soft X-ray band the spectrum is well described by the combination of a power law continuum and a thermal plasma with $kT=0.15 \text{ keV}$ (see Table 2). In Table 5 we

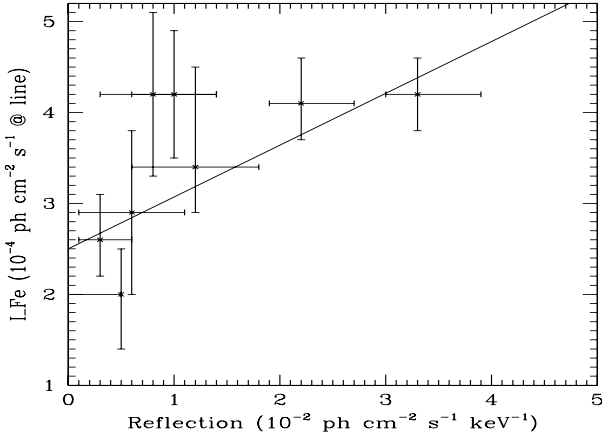


Fig. 6. The flux of the Iron line is plotted as a function of the Compton reflection component. We plot also the result of a linear fit

Table 5. Flux in 0.1–1 keV energy range. We report the total flux and that of the thermal and power law component. All the values are corrected for Galactic absorption.

Period	F^{tot}	F^{therm}	F^{scatt}
J96L	6.6	1.4	5.1
D96	6.6	1.2	5.4
J99L1	6.7	2.3	4.4
J99H	6.8	3.0	3.8
J99L2	5.4	0.6	4.8
D00	4.7	0.7	4.0
D01	8.1	1.6	5.5

Note: Flux corrected for Galactic absorption, in 10^{-12} erg $\text{cm}^{-2} \text{s}^{-1}$. The J96H state is not reported because the missing of soft X-ray data from LECS (see Section 2).

report the flux of these two components in the 0.1–1 keV range. The total flux in this range is dominated (≈ 80 per cent) by a constant power law with $F(0.1 - 1 \text{ keV}) \approx 5 \times 10^{-12} \text{ erg cm}^{-2} \text{s}^{-1}$, the remaining being attributed to the thermal component. We have computed the expected flux of the variable absorbed continuum in this energy range, finding that it is at most 1.5 per cent of the total. The only exception is the soft spectrum D01 where there is a contribution of the intrinsic continuum in 0.1–1 keV due to the effect of low absorption (see Table 2).

5. Discussion

5.1. The primary emission from the innermost region

The intrinsic continuum of NGC 4151 is well described by a power law with an exponential cut-off. The values of the high energy cut-off we found in the different flux level states are all consistent with the values observed in the Sy 1s by *BeppoSAX* (Perola et al. 2002).

This, together with the measure of the Compton reflection features that perfectly match with the averaged values observed in Sy 1s (Nandra & Pounds 1994), suggests that NGC 4151 is an intrinsically average Seyfert 1 galaxy (Zdziarski et al. 2002). The phenomenological model we employed to fit the intrinsic continuum (i.e. power-law with high energy cut-off), is a good description of a two-phase model involving a hot corona emitting medium-hard X-rays by Comptonization and a cold optically thick layer (the disk) that provides the soft photons to Comptonization (Haardt & Maraschi 1991; Haardt, Maraschi & Ghisellini 1997). While the dual absorber is the main driver of the observed variability in 2–10 keV, we find small amplitude of intrinsic variations above 10 keV, that can be due to a variation of $\Delta\Gamma \approx 0.2$, according to the correlation Γ vs $F_{2-10\text{keV}}$ (Perola et al. 1986). Assuming a distance of 13 Mpc for the source, and a black hole mass of $4 \times 10^7 M_\odot$ we find that the ratio $L_{0.1-200\text{keV}}^{\text{unabs}}/L_E$ between the unabsorbed luminosity and the Eddington luminosity is in the range 0.002–0.006 in the lowest (D00) and highest (J99H) state respectively. The accretion is taking place in a sub Eddington regime.

5.2. The narrow iron line and the reprocessing region: NLR and molecular torus

The energy of the narrow line as determined from the average of all *BeppoSAX* observations is $(6.40 \pm 0.06) \text{ keV}$, i.e. consistent with fluorescence by cold iron. During our observations, the line flux shows evidence of variations (see Table 4). We find that the flux of the line is dependent upon the normalization of the reflection component, and that it attains a non-zero value ($I = (2.5 \pm 0.3) \times 10^{-4} \text{ ph cm}^{-2} \text{s}^{-1}$) when the reflection is absent (in Figure 6 we plot the flux of the iron line as a function of the reflection amplitude). This suggests that the line is made up by two components. We first discuss the origin of the component at zero reflection. Our result indicates that this component is consistent with being constant, thus suggesting an extended origin. In addition, it should be produced by an optically thin gas. The flux we derive for this component is remarkably similar to the spatially resolved line emission region observed by *Chandra* (Ogle et al. 2000, $I = (1.8 \pm 0.2) \times 10^{-4} \text{ ph cm}^{-2} \text{s}^{-1}$). This region is coincident with the NLR, also in agreement with our conclusion of an optically thin gas.

The equivalent width of iron line in the case of an optically thin medium illuminated by an isotropic continuum is given by (e.g Inoue 1989; Piro 1993):

$$EW \approx 100 \frac{N_H}{10^{23} \text{ cm}^{-2}} \left(\frac{Z}{Z_\odot} \right)_{Fe} \frac{\Delta\Omega}{4\pi} \text{ eV} \quad (1)$$

where $\Delta\Omega/4\pi$ is the net solid angle covered by the medium (equal to the angular extension of the region $\Delta\Omega^*$ multiplied by f_{cov}). We can estimate the column density of the NLR $N_H = fRn$, by adopting the typical values derived from optical observations of the size

$R \approx 1$ kpc, density ($n \approx 200 - 1000 \text{ cm}^{-3}$) and filling factor ($f \approx 10^{-4}$; e.g. Robinson et al. 1994). By substituting these values in eq.(1) we derive an $EW \sim 0.1 - 0.3 \text{ eV}$ that is 2 orders of magnitude lower than observed (100-200 eV see Table 2). One possibility is that the ionizing flux is emitted anisotropically. Penston et al. (1990) showed that the ionizing flux needed to produce the observed optical and UV line emission had to be about 10 times stronger than that observed. Explanations for this excess include an anisotropic radiation field. But even in such a case, the expected EW would be lower of the observed value by a factor of 10. The presence of a system of clouds with higher density ($n \approx 10^6 \text{ cm}^{-3}$) can provide a more appealing explanation. In this hypothesis the column density of NLR would be $N_H \sim 3 \times 10^{23} \text{ cm}^{-2}$, then from eq. 1 we get an equivalent width $EW \sim 200\text{--}300 \text{ eV}$, that is in good agreement with the values we found. Spectral diagnostics of narrow lines in a sample of Seyfert nuclei that includes NGC 4151, reveals the presence of low density ($n \lesssim 10^4 \text{ cm}^{-3}$) and high ($n \gtrsim 10^6 \text{ cm}^{-3}$) density clouds (Stasińska 1984). Moreover, imaging of the NLR of NGC 4151 with *HST* shows the presence of regions whose density is likely to be enhanced by the shock compression of the ejected radio material (Winge et al. 1997).

Let us now discuss the line component that is correlated with the reflection normalization, characterized by $I = (0.57 \pm 0.17) \times 10^{-2} A_{\text{refl}} \text{ ph cm}^{-2} \text{ s}^{-1}$ (see Figure 6). The line produced by reprocessing by a cold thick medium has an intensity $I \approx 8 \times 10^{-3} G Y [(Z/Z_{\odot})_{\text{Fe}}] A_{\text{refl}} \text{ ph cm}^{-2} \text{ s}^{-1}$ where G is a function depending on the geometry, and is equal to ≈ 1 (substantially independent on the inclination angle) for simple configurations like a planar disk (Matt, Perola & Piro 1991) $Y[(Z/Z_{\odot})_{\text{Fe}}]$ describes the non-linear dependence of the line EW upon the iron abundance. For $(Z/Z_{\odot})_{\text{Fe}} = 2$, the case of NGC 4151, it is $Y = 1.6$ (Piro 1993), and the line flux should be $I \approx 1.2 \times 10^{-2} G A_{\text{refl}} \text{ ph cm}^{-2} \text{ s}^{-1}$, remarkably similar to the observed one for $G \approx 0.5$. Values of G less than unity are expected in a geometrically and optically thick torus, where the reprocessing takes place mostly in the inner wall, i.e. in a cylindrical or conical geometry. This is due to the “secondary illumination” effect, produced by photons emerging from the wall at angles that intercepts the wall again. This effect enhances the efficiency of reprocessing and does it more for the photons of the reprocessed continuum than for those in the line, because a 6.4 keV photon has a high probability to be absorbed. For example, if the disk is in a conical configuration with an opening angle of 45° , $G \approx 0.5$ (Matt, Perola & Piro 1991).

We now discuss the origin of the variability of the reflection component and the associated iron line. This could be due either to a variation of the illuminating continuum or to a change of the geometry of the reprocessing region. We recall that the intensity of the reflection decreases on a time scale of years by a factor of two or more from 1996 to 2000-2001 (see Table 4). The size of the reprocessing

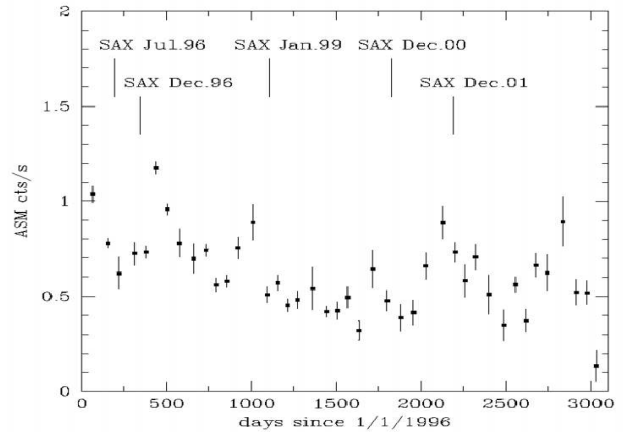


Fig. 7. Light curve in 1.5–10 keV of NGC 4151 from ASM aboard *RXTE*. Each bin is the flux averaged on 60 days.

region is therefore to be of the order of light-years. The intensity of the reflection component thus traces the level of the illuminating continuum averaged and delayed over a time scale of \approx year. We have therefore looked into the historical light curve of NGC 4151, to search for evidence of long time scale variability. In Figure 7 we report the light curve as observed by the ASM aboard of *RXTE*. Each point is the average flux over 2 months. The source shows a systematic decrease in its intensity by almost a factor of two from 1996 to 2000, consistent with the observed reflection variability.

The most obvious candidate for the reprocessing region is a thick torus whose inner walls are at \approx light years away from the central source. Taking then into account the line and reprocessing intensities we estimate¹ that the distance of the inner region of the torus should be $\approx 3 - 4$ times its height. The ionizing continuum would therefore emerge from the torus within a cone of opening angle of $\approx 70^\circ$, in agreement with the estimation based on the extended Narrow Line Region made by (Pedlar et al. 1983; Robinson et al. 1994). Finally we note that the variability of the reprocessing component could alternatively be explained by a change of the height of the torus.

5.3. The X-ray absorbers and the BLR

BeppoSAX observations of NGC 4151 show the presence of a complex absorber system. In particular the intrinsic continuum is absorbed by a cold gas that partially obscures the central source and by a second uniform warmer gas. Our analysis shows evidence of variations in the status of

¹ A precise determination of the geometry of the reprocessor goes however beyond the scope of this paper. It would require detailed computations, that should take into account the non-linear effect of secondary illumination, the solid angle subtended by the inner surface of the torus towards the X-ray source and their exposed area towards the observer.

the cold absorber on time scales of the order of the day and of the warm gas on longer time scale. Variations of the covered component can be produced if the cold medium is made up of clouds passing in the line of sight towards the central source (Reichert, Mushotzky & Holt 1986). If we identify these clouds with the BLR, from the typical velocity of $\approx 10^4 \text{ km s}^{-1}$, we derive that the size of the central source $R \approx 10^{14} \text{ cm}$. This would correspond, for $R \approx 10$ Schwarzschild radii, to a black hole mass of $4 \times 10^7 M_\odot$, consistent with independent estimations (Clavel et al. 1987; Wandel, Peterson & Malkan 1999). If the cloud velocity is due to the orbital motion, we derive that the distance of the clouds is a few light days, consistent with the size of the inner BLR in NGC 4151 (Clavel et al. 1987).

In our fit we have associated the warm stage with a uniform screen covering the source. In doing so we are guided by the arguments put forward by Warwick et al. (1995) to solve the discrepancy between the X-ray and UV measurements of absorption. Upper limits on UV extinction (Kriss et al. 1992) correspond to a column of $< 8 \times 10^{20} \text{ cm}^{-2}$ assuming a standard gas-to-dust ratio. This compares to X-ray columns of $10^{22} - 10^{23} \text{ cm}^{-2}$. In our case, the level of photoionization is such that a substantial fraction of light elements as H, He and C are ionized (e.g. Krolik & Kallman 1984), and therefore their absorption which is predominant in the UV range is reduced to a level compatible with UV measurements. We therefore associate the uniform absorber to the warm medium, while the patchy absorber is in a cold (neutral) stage.

Let us now characterize this warm medium we associated to the UV line absorbing system (Kriss et al. 1992). From the relationship $\xi = L/nR^2 \approx 10 \text{ erg cm s}^{-1}$, with $L_{0.1-200\text{keV}} \approx 3 \times 10^{43} \text{ erg s}^{-1}$ and the lower limit on the density $n \gtrsim 10^{9.5} \text{ cm}^{-3}$ derived by UV observations, we obtain that the size of this region should be $R \lesssim 10^{17} \text{ cm}$. This is consistent with the upper limit derived from the X-ray variability ($R \lesssim 10^{18} \text{ cm}$) and the requirement that the medium be external to the BLR ($R \gtrsim 10^{16} \text{ cm}$). In conclusion, our data are fully consistent with the scenario in which the ionized X-ray absorber coincides with the system responsible of UV absorption lines. This system is composed by many clumps of dense material covering the broad line region, and produced by an outflow of the broad-line clouds (Kriss et al. 1992).

The substantial decrease of the warm and cold absorbing gas in D01 together with the evidence, in the same spectrum, of an absorption feature at $\sim 8.5\text{-}9 \text{ keV}$ suggests the presence of a multi-phase ionized absorber. This topic is widely discussed in Piro et al. (2005).

5.4. Low energy diffuse components: scattering and thermal

The low energy emission in NGC 4151 remains constant on time scales of the order of years, indicating an extended

emission. We reproduced the soft X-ray spectrum with two components. One, dominated by emission lines, which is well fitted by a thermal plasma with $kT \approx 0.15 \text{ keV}$ with abundances comparable to solar. This is in agreement with *Chandra* observations (Ogle et al. 2000) that demonstrated that most of the soft X-ray flux is extended and dominated by lines from a photoionized and collisionally ionized plasma. The other component is a power law with a normalization $\approx 3 - 10$ per cent (see Table 3) of that of the hard power law, which is likely to be produced by electron scattering of the central continuum, as in the case of Seyfert 2 galaxies (Antonucci 1993; Matt et al. 1997). The fraction of this component in respect to the continuum is strongly dependent from the intrinsic flux. We expect the scattered fraction increase when the source flux decreases if the nuclear continuum is scattered into our line of sight. Weaver et al. (1994a) in *ASCA* observation of NGC 4151 found a fraction scattered of 3–4 per cent for the high state and 5–6 per cent for the low state. In our *BeppoSAX* observations the upper value of the ratio $A_{\text{scatt}}/A_{\text{IC}} \approx 10$ per cent is obtained in the D00 spectrum when the continuum level was lower in respect to the other states.

6. Conclusions

In this paper we presented the broad-band (0.1–200 keV) *BeppoSAX* spectrum of NGC 4151. The source was observed 5 times from 1996 to 2001 with durations ranging from a day to four days. We find that the spectrum is complex characterized by several components. The continuum emission is well reproduced by a cut-off power law.

At energies less than 5 keV the continuum is strongly obscured by a dual absorber: a cold component, that we associated with the BLR clouds orbiting around a central source with a black hole with a mass of $4 \times 10^7 M_\odot$, characterized by $N_{\text{H}} \approx 1.5 \times 10^{23} \text{ cm}^{-2}$, a covering fraction $f_{\text{cov}} = 0.3\text{--}0.7$ and variable on time scales of days to years, and a second warmer uniform screen (with $N_{\text{H}} = (1 - 8) \times 10^{22} \text{ cm}^{-2}$, variable on time scales of months-years), photoionized by the continuum emission and that we argue to be coincident with the UV absorbing region.

The low energies spectrum is reproduced by a combination of a two components, which are not absorbed by the cold and warm gas: a thermal one and a power law with the same slope of the intrinsic continuum but with the intensity which is a few per cent.

During our observations the source shows strong time variability energy dependent in time scales ranging from hours to years. In 0.1–2 keV it did not show any variability, while in 2–10 keV the variation was up to a factor of eight at 3 keV and three at 10 keV. In the PDS energy range (13–200 keV) the larger amplitude of variation was of a factor of three. We found that in 2–10 keV most of the spectral variability can be attributed to a variation of the absorbers. Intrinsic spectral changes can explain some of the smaller amplitude spectral variability above 10 keV.

We detected a Compton reflection component at high energy and the iron line at 6.4 keV. The intensity of the reflection component is significantly different from zero in 1996 while it disappears in 1999 and later (2000–2001). The size of this region, implied by the variability argument, as well as its optical thickness argue for an association with a geometrically and optically thick torus similar to that of Seyfert 2 galaxies. The study of the historical light curve of NGC 4151 suggests that the reflection component traces the level of the illuminating continuum averaged and delayed over a time scale of \approx year. We found that the iron line flux is well described by two components: one is correlated with the reflection intensity and is associated with the torus, the other is constant $I = (2.5 \pm 0.3) \times 10^{-4} \text{ ph cm}^{-2} \text{ s}^{-1}$ (in very good agreement with *Chandra* measurement). This component has to be produced in a diffuse optically thin gas, as confirmed by *Chandra* observations that have shown that about 70 per cent of the line is extended over a size of $\approx 1 \text{ kpc}$ coincident with the extended NLR.

Acknowledgements. The authors wish to thank the referee A. Zdziarski for constructive criticisms which have greatly improved the paper. A.D.R. acknowledge financial contribution from ASI-INAF I/023/05/0.

References

- Anders, E., & Grevesse, N. 1989, *GeCoA*, 53, 197
- Antonucci, R.R. 1993, *ARA&A*, 31, 473
- Beckmann, V., Shrader, C.R., Gehrels, N., et al. 2005, *ApJ*, 634, 939
- Boella, G., Butler, R.C., Perola, G.C., Piro, L., Scarsi, L., Bleeker, J.A.M. 1997, *A&AS*, 122, 299
- Clavel, J., Altamore, A., Boksenberg, A., et al. 1987 *ApJ*, 321, 251
- De Rosa, A., Piro, L., Fiore, F. 2002a, *A&A*, 387, 838
- De Rosa, A., Piro, L., Matt, G., Perola, G.C. 2004, *A&A*, 413, 895
- Done, C., Mulchaey, J.S., Mushotzky, R.F., Arnaud, K.A. 1992, *ApJ* 395, 275
- Done, C., Madejski, G.M., Zycki, P.T. 2000, *ApJ*, 536, 213
- Fabian, A.C., Iwasawa, K., Reynolds, C.S., Young, A.J. 2000, *PASP*, 112, 1145
- Fiore, F., Guainazzi, M., & Grandi, P. 1999, *Cookbook for BeppoSAX NFI Spectral Analysis*
- Haardt, F., & Maraschi, L. 1991, *ApJ*, 380, L51
- Haardt, F., Maraschi, L., & Ghisellini, G. 1997, *ApJ*, 476, 620
- Kaspi, S., Brandt, W.N., Netzer, H., et al. 2001, *ApJ*, 554, 216
- Holt, S.S., et al. 1980, *ApJ*, 241, L13
- Inoue, H. 1989, *proc. of 23rd ESLAB symposium in X-ray astronomy*, Bologna, Sep.13-20 1989, p.783 (ESA SP-296)
- Krolik, J.H., & Kallman, T.R., 1984, *ApJ*, 286, 366
- Kriss, G.A., Davidsen, A.F., Blair, William P., et al. 1992, *ApJ*, 392, 485.
- Matt, G., Perola, G.C., & Piro, L. 1991, *A&A*, 247, 25
- Matt, G., Guainazzi, M., Frontera, F., et al. 1997, *A&A*, 325, L13
- Matt, G., Guainazzi, M., Perola, G.C., et al. 2001, *A&A*, 377, L31
- Magdziarz, P., & Zdziarski, A.A. 1995, *MNRAS*, 273, 837
- Nandra, K., Pounds, K.A. 1994, *MNRAS*, 268, 405
- Nandra, K., Le, T., George, I., et al. 2000, *ApJ*, 544, 734
- Nicastro, F., Piro, L., De Rosa, A., et al. 2000, *ApJ*, 536, 718
- Ogle, P.M., Marshall, H.L., Lee, J.C., & Canizares, C.R. 2000 *ApJ*, 545, L81
- Page, K., Pounds, K., Reeves, J., O'Brien, P.T. 2002, *MNRAS*, 330, L1
- Pedlar, A., Kukula, M.J., Longley, D.P.T., et al. 1993, *MNRAS*, 263, 471
- Penston, M.V., Robinson, A., Alloin, D., et al. 1990, *A&A*, 236, 53
- Perola, G.C., Piro, L., Altamore, A., et al. 1986, *ApJ*, 306, 508
- Perola, G.C., Matt, G., Cappi, M., Fiore, F., Guainazzi, M., Maraschi, L., Petrucci, P.O., Piro, L. 2002, *A&A*, 389, 802
- Petrucci, P.O., Haardt, F., Maraschi, L., et al. 2000, *ApJ*, 540, 131
- Piro, L. 1993, *proc of UV and X-ray spectroscopy of astrophysical and laboratory plasmas*, Berkeley Feb.3-5 1992, E.H. Silver & S. M. Kahn ed.s, p. 448 (Cambridge Univ. Press)
- Piro, L., Scarsi, L., & Butler, R.C. 1995, *Proc. of SPIE*, 2517, 169
- Piro, L., De Rosa, A., Matt, G. and Perola, G.C. 2005, *A&AL*, 441, L13
- Pounds, K.A., Warwick, R.S., Culhane, J.L., de Korte, P. 1986, *MNRAS* 218, 685
- Pounds, K., Reeves, J., O'Brien, P., et al. 2001, *ApJ*, 559, 181
- Reeves, J.N., Turner, M.J.L., Pounds, K.A., et al. 2001, 365, L134
- Reichert, G.A., Mushotzky, R.F., & Holt, S.S. 1986, *ApJ*, 303, 87
- Robinson, A., Vila-Vilaro, B., Axon, D.J., et al. 1994, *A&A*, 291, 351
- Schurch, N.J., & Warwick, R.S. 2002, *MNRAS*, 334, 811
- Schurch, N.J., Warwick, R.S., Griffiths, R.E., Sembay, S. 2003, *MNRAS*, 345, 423
- Stasińska, G. 1984, *A&A*, 135, 341
- Svensson, R. 1994, *ApJS*, 92, 585
- Tanaka, Y., Nandra, K., Fabian, A.C., et al. 1995, *Nature*, 375, 659
- Ulrich, M.-H., 2000, *A&A Rev*, 10, 135
- Vaughan, S., & Edelson, R. 2001, *ApJ*, 548, 694
- Wandel, A., Peterson, B.M., & Malkan, M.A. 1999, *ApJ*, 526, 579
- Warwick, R.S., Done, C., & Smith, D.A. 1995, *MNRAS*, 275, 100
- Weaver, K., Mushotzky, R.F., Arnaud, K.A., et al. 1994a, *ApJ*, 423, 621
- Weaver, K., Yaqoob, T., Holt, S.S., et al. 1994b, *ApJ*, 436, L27
- Winge, C., Axon, D.J., Macchetto, F.D., & Capetti, A. 1997, *ApJ* 487, L121
- Yaqoob, T., & Warwick, R.S. 1991, *MNRAS*, 248, 773
- Yaqoob, T., Warwick, R.S., Makino, F., et al. 1993, *MNRAS*, 262, 435
- Yaqoob, T., George, I.M., Nandra, K., et al. 2001, *ApJ*, 546, 759
- Zdziarski, A.A., Johnson, W.N., & Magdziarz, P. 1996, *MNRAS* 283, 193
- Zdziarski, A.A., Leighly, K.M., Matsuoka, M., Cappi, M., Mihara, T. 2002, *ApJ*, 573, 505
- Zdziarski, A.A., Lubiński, P., Gilfanov, M., Revnivtsev, M. 2003, *MNRAS*, 342, 355